ADVANCED ELECTRONIC MATERIALS
www.advelectronicmat.de

Strategies to Control the Relaxation Kinetics of Ag-Based Diffusive Memristors and Implications for Device Operation

Solomon Amsalu Chekol, Stephan Menzel, Rainer Waser, and Susanne Hoffmann-Eifert**

Diffusive memristors based on volatile electrochemical metallization (v-ECM) devices are of broad interest for applications in emerging memory technologies and neuromorphic computing areas due to their interesting features such as thresholding, self-relaxation, and energy-efficient switching behaviors. Recently, the nonlinear threshold kinetics and the correlation of filament formation and growth with its relaxation behavior are uncovered from a physical perspective. However, the complexity of the diffusive memristors' behavior might still hamper a straight transfer into emerging computing applications. Facing this challenge means going beyond the single device level and understanding the impact of other circuitry elements for further optimization of device operation. In this work, the effect of a series resistor on the switching dynamics of Ag/HfO_2/Pt diffusive memristor devices by deploying various programming schemes with different resistances is investigated. Furthermore, all results and their implications on devices' operation are compressively discussed. These findings help to further advance the optimization of the operating condition of diffusive memristors.

1. Introduction

The amount of data that is being created every day is growing astronomically and is expected to keep increasing not only in volume but also in complexity. Processing such big and complex data efficiently requires new computing concepts. So far, in traditional von-Neumann architecture, the computing unit and the memory are physically separated, leading to high energy consumption caused by charging and discharging of the load lines and limitations in data transfer rate, often referred to as the von-Neumann bottleneck.[1] To overcome this, emerging novel architectures are discussed such as neuromorphic computing concepts that use memristive devices to mimic certain functionalities of the biological brain.[2,3–7] Memristive devices enable voltage-controlled resistance change under external stimuli, and they are highly promising for use in neuromorphic applications thanks to their low power consumption,[8] 3D integration capability,[9] and scalability.[10–16] Among others, electrochemical metallization cells (ECMs) are an attractive class of memristive devices. Particular in nonvolatile ECMs the formation and rupture of a metallic conductive filament made of Ag or Cu inside an electrolyte matrix is responsible for the switching between a high-resistive state (HRS) and a low-resistive state (LRS).[17–22] A wide range of electrolyte materials have been used including pure ion conductors such as Ag_2S[11] and AgI,[23] mixed ion-electron conductors (MIEC) such as Ge_xSe_{1-x},[24,25] and oxide insulators such as SiO_2,[26,27] TiO_2[28] and HfO_2.[29] The stability of the conductive filament depends on various factors such as the filament size and morphology, type of the active species, the switching matrix, and other external factors like temperature and bias voltage. Stable filaments can provide a long retention time, up to 10 years,[30,31] for the ECM cell, meaning that the programmed state is nonvolatile. Such nonvolatility can be achieved by either engineering the material stack, for example, using Cu as an active electrode, or by programming the device electrically to a higher current level. While the programming from HRS to LRS is triggered by applying a certain SET voltage of V_{SET}, a RESET voltage of V_{RESET} with the opposite polarity is required to erase the programmed state. Such devices have been researched intensively for storage[32–34] and neuromorphic computing applications.[35–38] On the other hand, ECM cells with an unstable filament, i.e., a device with a much shorter filament lifetime, are classified as volatile ECMs (v-ECMs) or diffusive memristors (DMs), and the lifetime of the filament is referred to as relaxation time.[39,40]

The switching behavior for the threshold-type SET of DMs is similar to that of non-volatile ECMs. In contrast, DMs do not require a RESET voltage as the filament is volatile and spontaneously self-ruptures if the voltage drops below the hold voltage V_{hold}.[39,41] The driving force for the self-relaxation

S. A. Chekol, S. Menzel, R. Waser, S. Hoffmann-Eifert
Peter Grünberg Institute (PGI 7 and 10) and JARA-FIT
Forschungszentrum Jülich GmbH
Wilhelm-Johnen-Straße, 52428 Jülich, Germany
E-mail: s.chekol@fz-juelich.de; su.hoffmann@fz-juelich.de
S. A. Chekol
RWTH Aachen University
Templergraben 55, 52062 Aachen, Germany
R. Waser
Institute of Materials in Electrical Engineering and Information Technology II
RWTH Aachen University
Sommerfeldstraße 24, 52074 Aachen, Germany
The ORCID identification number(s) for the author(s) of this article can be found under https://doi.org/10.1002/aelm.202200549.

DOI: 10.1002/aelm.202200549

behavior can originate from surface energy minimization or surface tension effects,[42–44] thermo-diffusion,[45] mechanical stress,[46] steric repulsion effect,[47] or a combination of some, depending on the nature of the filament and the surrounding switching matrix.

DMs are very attractive for a variety of interesting applications including access devices for memristive crossbar arrays,[48–50] artificial neuron and synaptic emulators in neuromorphic computing,[39,40,51,52] and true random number generators (TRNGs) in network security.[53] All these applications leverage the thresholding and self-relaxation behavior, highlighting the temporal behavior of such devices of great importance. Recently, we reported on the correlation between the SET process and relaxation behavior in DMs using an $Ag/HfO_2/Pt$ system.[54] By deploying different programming schemes we showed the strong dependence of both SET (t_{set}) and relaxation times (t_r) on programming pulse amplitude (V_p) and duration (t_p), discussed voltage-dependent filament growth mechanisms, and outlined ways to tune t_{set} and t_r. It turned out that successful utilization of DMs in complex circuits, whether for storage applications or in the emerging field of neuromorphic computation, will depend on a predictive and controllable threshold and relaxation behavior, especially for DMs being integrated into a larger circuitry. For example, in a one-selector one-resistor (1S1R) configuration the DM-based access device is connected in series with the adjacent memory cell.[49] The memory cell can be in HRS or different LRS states, depending on the previously programmed state, thus, effectively behaving as a series resistor (R_{series}) towards the DM cell. It has been previously shown that R_{series} can greatly influence the switching kinetics and performance of non-volatile memristive devices.[55–57] Therefore, understanding the influence of a series resistance on the switching kinetics of DMs is equivalently important.

In this study, the effect of a series resistance R_{series} on both the SET and relaxation kinetics of $Ag/HfO_2/Pt$ DM devices is presented. Different R_{series} of 50 kΩ, 100 kΩ, 560 kΩ, and 1 MΩ in combination with programming schemes of varied voltage amplitude (V_p) and pulse width (t_p) were deployed to investigate the influence of R_{series} on the SET and relaxation times of t_{set} and t_r, respectively. Extracting both times from the same transient curve allowed us to analyze and evaluate the effect of R_{series} on t_{set} and t_r under the same programming condition.

2. Results and Discussion

2.1. Ag/HfO_2-Based Filamentary Diffusive Memristor Device and Characteristics

Figure 1a shows the stack and structure of the fabricated device. All cells were structured in a microcrossbar-type configuration with an area of $(3.0 \pm 0.2)\ \mu m^2$. An about 3 nm thick HfO_2 insulating layer grown by plasma-enhanced atomic layer deposition (PE-ALD) on a Pt bottom/counter electrode is used as the electrolyte. A Pt-capped Ag top electrode served as the active metal layer for cation supply. As shown in Figure 1b, the fabricated DM cell exhibits a volatile switching characteristic for a wide range of compliance currents (I_{CC}) up to 1 mA with excellent features such as ultra-low leakage current, low threshold voltage (V_{th}), large on/off ratio and an abrupt transition from the HRS to the LRS. These properties together with the unique self-relaxing behavior make this type of device a promising energy-efficient solution for applications in storage memory and neuromorphic computing areas. A one-time forming process is initially required on the pristine device with a relatively higher forming voltage (V_F) than the V_{th}. During this process, ionized Ag atoms (Ag^+) are introduced into the HfO_2 switching matrix and form a conductive filament that bridges the two electrodes electrically. Typical forming curves of the fabricated devices can be found in Figure S1 (Supporting Information). Once the forming process is performed the relaxation and reformation of the conductive filament are responsible for further switching cycles, thus requiring a much smaller switching voltage of V_{th}. A statistical analysis of V_{th} with data collected from 10 random cells and 100 cycles each shows the reliable switching of the fabricated devices (Figure 1c). Quasi-static I–V curves of the device in series with different resistors R_{series} of 50 kΩ, 100 kΩ, 560 kΩ, and 1 MΩ are shown in Figure 1d.

A typical current response of the device under a voltage pulse with amplitude V_p of 1.6 V and duration t_p of 10 µs is shown in **Figure 2**a. The measurement setup used for all transient measurements in this work is shown in Figure 2b. Upon the application of the voltage pulse, the device current abruptly rises after a certain time period of t_{set} marking the onset of the switching from HRS to LRS (Figure 2c). When the programming is finished and the voltage is set to the read voltage V_{read}, the device current spontaneously relaxes back to the HRS within a definite time period of t_r (Figure 2a). Figure 2d presents a temporal response of an $Ag/HfO_2/Pt$ device acquired using a 1.6 V/10 µs programming pulse and two different R_{series} of 50 and 100 kΩ. As can be seen in the inset of Figure 2d, different relaxation times are observed for different R_{series} values and this will be discussed in detail in the subsequent sections.

2.2. SET Kinetics of a Diffusive Memristor in Series with a Resistor

Fast programming times are among the top desires for efficient and improved performance of emerging memristor-based technologies. In this regard, understanding the switching kinetics and exploiting ways to control and/or improve the switching times of DMs is vitally important. The dependence of t_{set} on the programming scheme has previously been studied by different research groups.[27,48,54,58,59] It has been shown that t_{set} exponentially decays with V_p. Considering the strong non-linearity in the dependence of switching times on the programming scheme, additionally, studying the effect of a series resistor on the switching kinetics could be very crucial to expanding the knowledge of such devices' behavior beyond the individual cell level and towards integration. In addition, compact models could be validated based on these small circuits.

To that end, four different SMD (surface mounted device) resistors with a value of 50, 100, 560 kΩ, and 1 MΩ were arranged in series with the DM device to investigate the impact of R_{series} on the t_{set}. The SMD resistors (COMP-CARD-System, NOVA Electronik GmbH) were introduced by inserting them into a

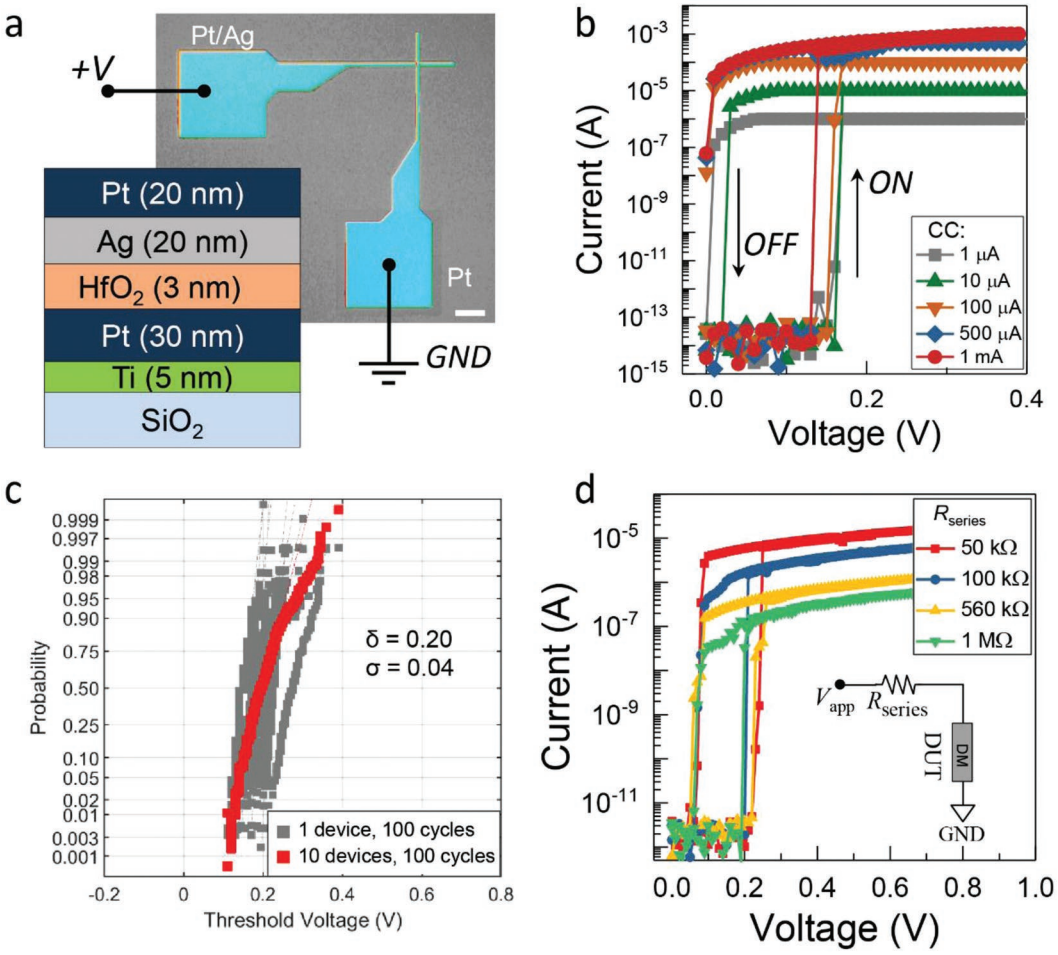

Figure 1. a) Schematic representation of the fabricated crossbar structure of an Ag/HfO_2/Pt device and a scanning electron microscopy photography from the top. Scale bar 10 µm. The voltage signal is applied to the Pt/Ag active electrode while the Pt counter electrode is grounded. b) Typical *I–V* sweeps measured on the same device under various compliance currents (I_{CC}), showing volatile switching up to 1 mA. c) Statistics of the threshold voltage collected from 10 devices and 100 cycles each at a sweep rate of 0.2 V s^{-1}, exhibiting uniform and reproducible switching. d) *I–V* sweep measurements performed on the same device with different series resistances. The inset shows the electrical connection during the measurement.

custom-built tungsten probe tip. The measurement setup used to collect the temporal responses is depicted in Figure 2c. We used a Keithley 4200 SCS Semiconductor Analyzer equipped with four 4225 PMUs and an integrated oscilloscope card (coupled with 50 Ω) with a bandwidth of 1 GHz. The input signal is applied to the Pt/Ag top electrode while the Pt counter electrode is grounded. Programming pulses of varied V_p and t_p ranging from 0.3 V to 2.2 V and 1 µs to 1 s, respectively, were applied to the cell. After the collection of data from different V_p and t_p combinations, the respective switching times t_{set} were extracted from the transient current response and plotted against V_p for different values of R_{series} (**Figure 3**a–d). Here, t_{set} is defined as the interval between the V_p maximum edge and the onset of the output current rise (Figure 2b). As expected, exponential decay of t_{set} with respect to V_p is obtained for all R_{series}. At low voltages, no change in the SET kinetics is observed for all R_{series}. However, at higher voltage (>1.0 V) splitting of the t_{set} with different R_{series} can be observed. As the R_{series} value changes from 50 kΩ to 1 MΩ, the t_{set} increases by almost two orders of magnitude, roughly from 30 ns to 1.3 µs (Figure 3e).

In general, a series resistor influences the switching performance of memristive switches by acting as a voltage divider element.[55] This becomes relevant if the value of the series resistor is not far away from the resistance of the memristive device. However, considering the extremely high resistance of the DM cell in the HRS (>TΩ, Figure S3 of the Supporting Information) compared to the largest R_{series} used (1 MΩ), we should not expect any influence of R_{series} on the t_{set}. This is true for $V_p < 0.9$ V but it fails for $V_p > 1.0$ V. Therefore, to understand the origin, the t_{set} values at the saturation regions were plotted against R_{series} (Figure 3f). Assuming the t_{set} values in the flat region (≈2.1 V) to represent an *RC*-time constant τ, the slope of a linearly fitted τ-R_{series} plot gives us the total parasitic capacitance C_p of the whole system using the simple equation $\tau = R_{series} \cdot C_p$. From the data in Figure 3f a value of $C_p = (1.15 \pm 0.05)$ pF is obtained. A typical memristive cell is basically a parallel plate capacitor with a thin oxide (dielectric) material. Considering the extremely high resistance in the HRS, the DM cell can, initially, act as an ideal capacitor (Figure S2 of the Supporting Information). Additionally, the parasitic capacitance

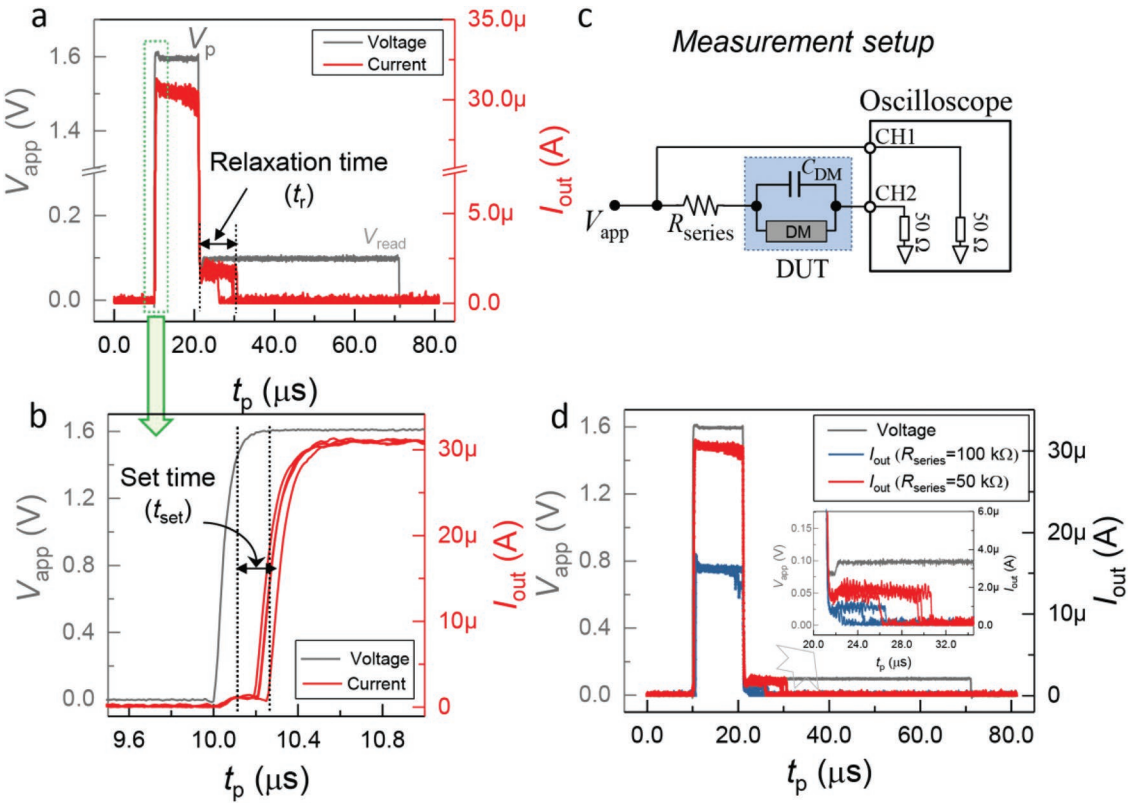

Figure 2. a) Typical transient pulse measurement of an Ag/HfO_2/Pt device under a 1.6 V/ 10 µs programming pulse followed by a 0.1 V/ 50 µs read pulse. A 50 kΩ series resistor R_{series} was used to limit the maximum current. Gray color: applied voltage (V_{app}); red color: output current signal (I_{out}). b) Magnified image of the box with the green broken line in (a). The definitions of t_{set} and t_r are shown in (b) and (a), respectively. c) The measurement setup used to carry out all transient pulse measurements in this work. d) Transient measurement under different series resistance. The inset shows the typical effect of a series resistor on the relaxation time. Gray color: applied voltage (V_{app}); red and blue colors: output current signal (I_{out}) for R_{series} of 50 and 100 kΩ, respectively.

of the measurement setup should be taken into account. Therefore, we performed a capacitance–voltage (*C*–*V*) measurement on the DM cell at 100 kHz and found a capacitance value of about 0.17 pF. This yields a mean dielectric permittivity value of the amorphous HfO_2 layer of about 19, close to the reported values between 18 and 25,[60–63] and a reasonable equivalent oxide thickness (EOT) of 0.6 nm for a 3 nm HfO_2 dielectric layer.[61,64] The rest of the parasitic capacitance is attributed to the measurement setup and all the electrical connections.

The observed limitation of the SET time is, thus, not due to an intrinsic physical property of the switching device stack, but by the charging time of the collective capacitance of the DM and measurement setup environment. Depending on the voltage regime, the SET event of the DM is controlled by three different processes involved during the switching. These are nucleation, electron transfer, and ion migration.[54,59,65] At low voltage regimes, nucleation dictates the switching process and, ultimately, t_{set} is determined by the nucleation time. At medium voltage regimes, the process is limited by electron-transfer reaction between the growing filament/metal electrode and metal/oxide interfaces. With further increase of the voltage, the ion migration also comes into play, in addition to the electron-transfer process. This third regime is referred to as a mixed electron-transfer- and ion-migration-limited regime. These three limiting processes define the final shape of the SET kinetics plot that provides t_{set} on a logarithmic scale as a function of V_p.

Figure 4 presents simulation results fitted to the experimental data using a model implemented recently.[54,59,65] The *RC*-time effect was introduced into the fitting by considering a time constant defined by (R_{series} · 1.15 pF). As can be seen in Figure 4a, the simulation nicely matches the experimental data. Details of the analytical model and all the fitting parameters used in the simulation can be found in the Supporting Information. Here, it should be noted that the capacitance effect can be mitigated and faster SET times can be achieved by reducing the parasitic capacitances of the measurement setup and further scaling the device area.[66] This is shown with simulation data as presented in Figure 4b. By assuming a C_p of only 1 fF, the effect of the R_{series} on t_{set} becomes negligible, and fast SET events with t_{set} of a few nanoseconds could be achieved.

2.3. Relaxation Kinetics of a Diffusive Memristor in Series with a Resistor

The relaxation process and the relaxation time, t_r, depend on the size and shape of the conductive filament that was formed during the SET process. A large and strong filament tends to take a longer time to rupture and a thin and fragile filament,

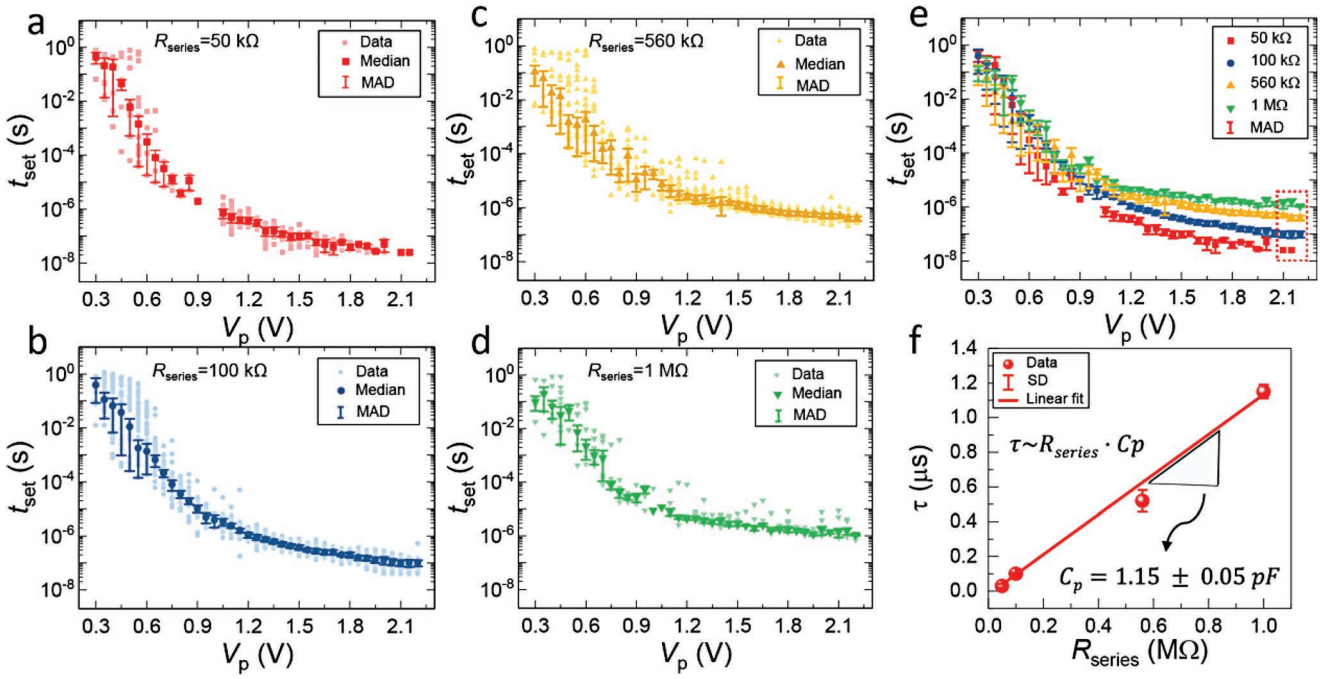

Figure 3. SET switching kinetics of Ag/HfO_2/Pt DM cells in series with different resistors of a) 50 kΩ, b) 100 kΩ, c) 560 kΩ, and d) 1 MΩ. The median values and median absolute deviations (MAD) of the experimental data are displayed using color-filled symbols and vertical lines, respectively. 20 measurements for every V_p/ t_p combination were performed and transient curves with a successful switching event were further analyzed and used for the plots. e) A plot of the median values of t_{set} as a function of V_p for the four different series resistors. f) SET times t_{set} taken from the red box marked region in (e) plotted against R_{series} provide the parasitic capacitance C_p.

on the other hand, ruptures rather fast. The filament formation process comprises two steps: nucleation and growth. Initially, at the early stage of filament formation, multiple filament seeds can be formed owing to the randomness of the nucleation process. However, due to the strong field dependence of the switching behavior, only a single "winning" filament further evolves during the growth process and bridges the two electrodes electrically. Consequently, the relaxation time will be dominated by the strength of this filament. Furthermore, the strength of the filament is determined by the programming condition during the SET process. Unlike the SET kinetics where t_{set} is determined at the closing of the filament, t_r depends on the final size of the filament. That means, not only V_p controls t_r but also t_p since continued growth of a conductive filament is possible throughout the entire pulse duration.[48,54]

A resistor in series to the DM can act as a current limiter and a voltage divider in the LRS, although the voltage divider effect depends on the R_{series} and the resistance of the cell.[56,57] Therefore, investigating the effect of R_{series} on the relaxation process and establishing any relationship between the two is important

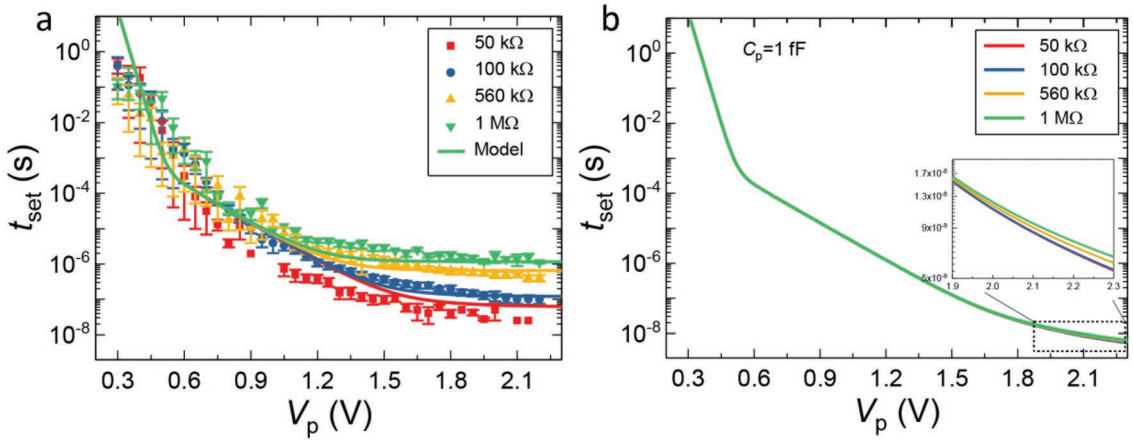

Figure 4. a) Analytical simulation of the SET kinetics of a DM in series with a resistor of different value R_{series} when an *RC*-time constant of the circuit is considered with C_p = 1.15 pF. b) Simulation data obtained with an assumed C_p value of 1 fF, showing faster switching times and negligible differences between the R_{series} values. The median and median absolute deviation (MAD) of the experimental data are displayed using color-filled symbols and vertical lines, respectively, and the simulation results are shown as solid lines.

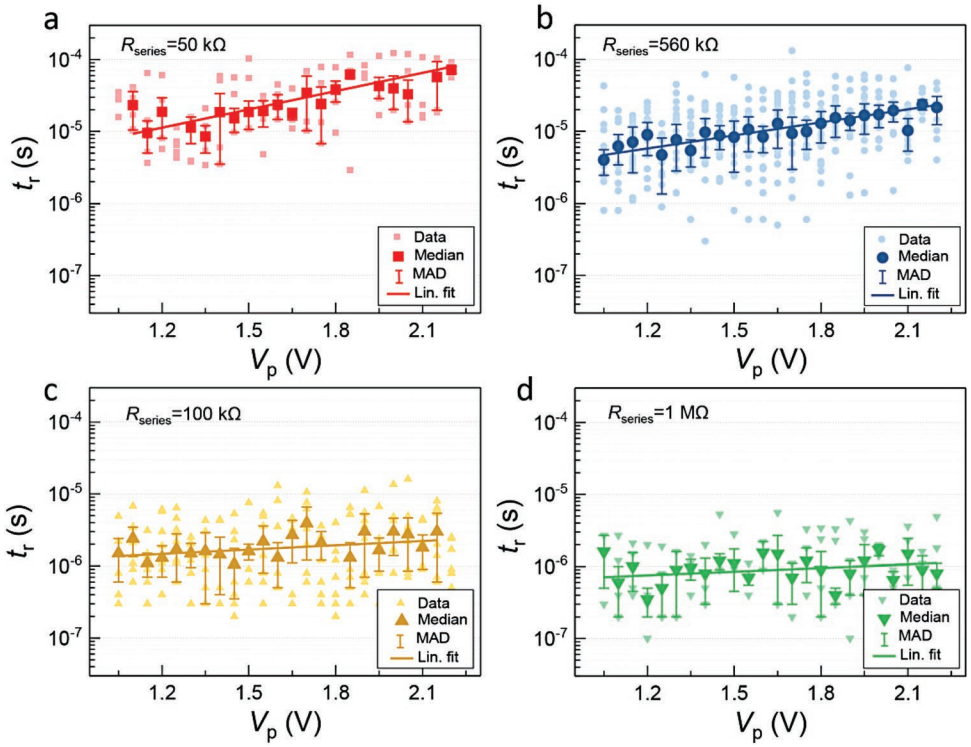

Figure 5. Relaxation kinetics plot of t_r as a function of V_p with a fixed t_p of 1 ms for different R_{series} of a) 50 kΩ, b) 100 kΩ, c) 560 kΩ, and d) 1 MΩ. The median and median absolute deviation (MAD) of the experimental data are displayed using color-filled symbols and vertical lines, respectively.

to further advance understanding and control of the relaxation dynamics of DMs.

To examine this, the relaxation times were extracted and analyzed from the same transient measurements used for the SET kinetics study. The relaxation time is defined as the time between where the voltage drops to the monitoring voltage V_{read} (V_{read} = 0.1 V) and where the output response current fully relaxes back to the initial state (Figure 2a). Data with a successful switching event and current relaxation to the HRS within the duration of the read pulse are considered for the analysis of t_r. Plots of t_r against V_p for different t_p of 1, 10, 100 µs, and 1 ms measured with R_{series} of 100 kΩ are shown in Figure S3a in the Supporting Information. As shown from the median data in Figure S3b (Supporting Information), the t_r changes by more than two orders of magnitude when the V_p and t_p change from 1.05 to 2.20 V and 1 µs to 1 ms, respectively.

To further investigate the effect of R_{series} on t_r, relaxation times with different R_{series} were extracted in the same way from the t_p of 1 ms. The results are presented in **Figure 5**. Three dependencies can be identified from the graphs in Figure 5: i) t_r strongly decreases as the R_{series} increases, ii) t_r increases as the voltage V_p increases, and iii) the slope in the $\log(t_r)$–V_p plot changes with varying R_{series} (**Figure 6**). In detail, (i), changing the R_{series} by a factor of 20, i.e., from 50 kΩ to 1 MΩ, results in a decrease of t_r by more than a decade at a given V_p. Values determined at V_p of 1.1 V and 2.1 V, give a decrease of t_r roughly from 10 µs to 700 ns and from 70 µs to 900 ns, respectively. In addition, (ii), a linear increase of $\log(t_r)$ with increasing V_p can be clearly observed for all four graphs. This is quite surprising considering that relaxation time is mainly determined by filament size and instability. According to the physical mechanisms contributing to the filament growth[54,59] the expected dependency is a decrease in t_r with increasing V_p. At low voltages where nucleation dominates the process, the growth is homogenous and a bulky filament is expected. However, with increasing voltage approaching the regimes controlled by electron-transfer and mixed (electron-transfer and ion-migration), the filament shape changes from relatively bulky to thick dendritic type, and finally tiny wire-like, respectively. In other words, as the V_p increases, the filament size keeps getting smaller. As a result, the relaxation process should become faster as V_p increases.

On the contrary, as shown in Figure 5, t_r increases as the voltage increases, while the incremental rate additionally depends on R_{series}. Supporting the experimental findings, previous reports on the relaxation behavior of DMs have claimed similar trends of rising relaxation time with increasing voltage.[49,67–69] The explanation for this apparent contradiction between the experimental data and the prediction from physics-based simulation can be traced back to the influence of the series resistance and residual voltage drop. In Figure 5, the relaxation times were extracted after the application of a defined voltage pulse of V_p and a fixed t_p (see Figure 2a). But this means that after the closure of the filament the device in LRS keeps being exposed to a fraction of the applied voltage for the remaining pulse time, (t_p – t_{set}). Once the filament is formed, any prolongation of the t_r due to a further filament growth is an effect of not only the V_p but also the t_p. This should not come as a surprise considering the strong dependence of t_r on t_p (Figure S3 in the Supporting Information). The residual voltage drop δV_p is a function of the resistance of the

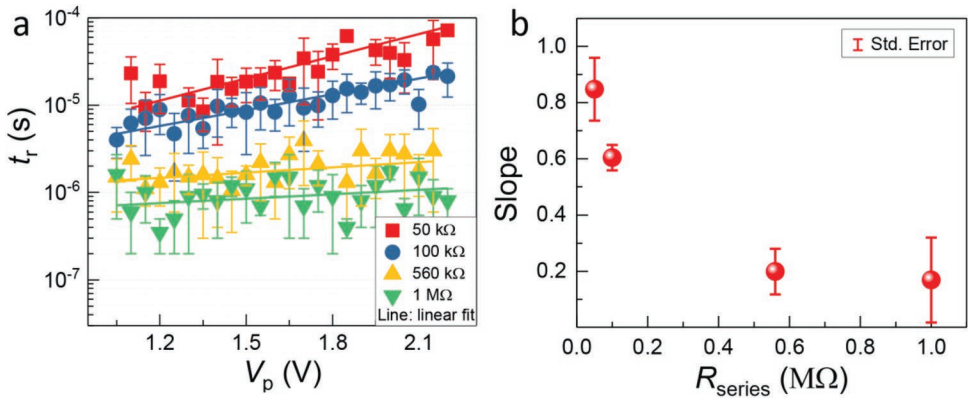

Figure 6. a) Median t_r for different R_{series} plotted against V_p. Median absolute deviation (MAD) is represented using vertical lines. b) Slopes extracted from (a) and plotted as a function of R_{series}.

device in LRS and the R_{series}. Furthermore, iii) Figure 6a shows more clearly the declining slope in the $\log(t_r)$–V_p dependence observed for increasing R_{series}. Quantitative data are provided in Figure 6b. From this study, it becomes obvious that the relaxation time of a DM device depends on the SET programming conditions, V_p and t_p (in relation to the SET kinetics), and the series resistance R_{series} in line with the DM. The role of R_{series} on the dependency of t_r from the programming pulse V_p for a given t_p will be discussed in detail in the next section.

2.4. Filament Growth and the Effect of Residual Voltage Drop

The filament growth mechanism and, ultimately, final filament size determine the relaxation duration of the DM cells.[54] This means the relaxation time is a reflection of the strength of the filament that was formed during the programming stage. This strength can be expressed in terms of the resistance of the cell. The cell resistance after programming mainly depends on the programming voltage amplitude and duration. The R_{series} reduces the voltage drop across the DM cell, V_{dm}, during the SET process eventually to a certain minimum voltage V_{min}, at which the driving force for resistance reduction of the DM cell becomes zero.[55,56] The V_{min} is connected to the kinetics of the device and can be traced from the asymptotic line of the SET kinetics curve at low voltage, i.e., equivalent to the V_{th} of the DM from sweep measurement (Figure 1b,c). Below V_{min} (in this case ≈ 0.10–0.15 V) the device does not switch regardless of the measurement time. However, for $V_{dm} > V_{min}$, the resistance of the DM cell R_{dm} will keep reducing until V_{dm} reaches V_{min}. The output current, I_{out}, during the SET process for a given t_p and V_p can be expressed by Kirchhoff's current law:

$$I_{out} = \frac{V_p}{R_{total}} = \frac{V_p}{R_{series} + R_{dm}} \quad (1)$$

Rearranging Equation 1 yields an expression for the cell resistance R_{dm} as a function of V_p, I_{out}, and R_{series}

$$R_{dm} = \left(\frac{V_p}{I_{out}}\right) - R_{series} \quad (2)$$

In **Figure 7**a, the total resistance R_{total} in the LRS is plotted as a function of the R_{series}. The cell resistance R_{dm} calculated by using Equation 2 and plotted against the programming voltage V_p for pulse duration t_p of 1 ms is presented in Figure 7b. From

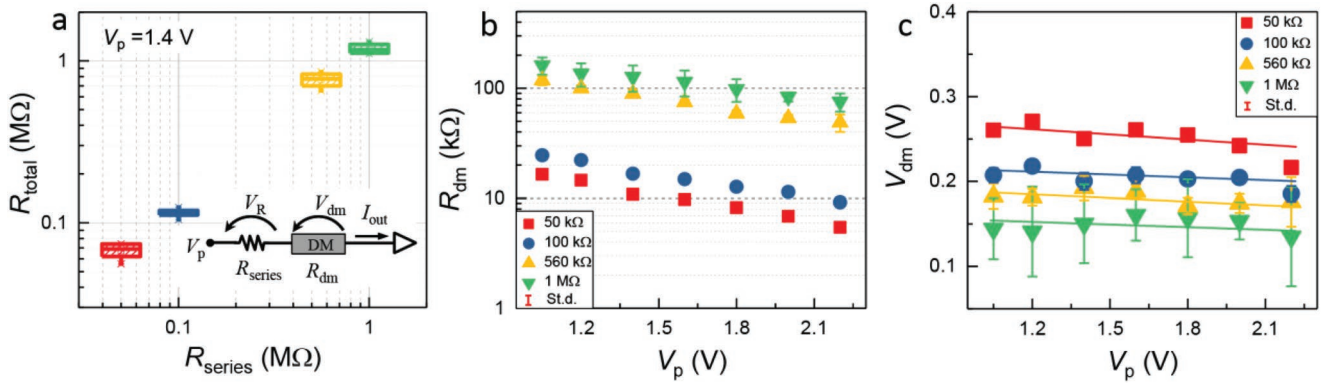

Figure 7. a) Total resistance calculated from the output current I_{out} of the transient curve in the LRS and V_p plotted as a function of R_{series}. The inset displays a schematic representation of the voltage divider effect between the DM and the series resistor. b) Device resistance R_{dm} and c) voltage drop across the device V_{dm} calculated using Equations 2 and 3 plotted as a function of V_p for different R_{series} values. The lines in (c) are a guide to the eye.

the result, two trends can be observed: i) R_{dm} decreases with V_p establishing an inverse relationship, and ii) R_{dm} increases as the value of the R_{series} increases. Furthermore, the voltage across the cell V_{dm} at a given t_p can be calculated from:

$$V_{dm}(t_p) = \left(\frac{R_{dm}}{R_{series} + R_{dm}}\right) \cdot V_p \quad (3)$$

Here it should be noted that both R_{dm} and V_{dm} of the cell also depend on the pulse duration t_p (Figure S4 in the Supporting Information). However, for simplicity data with a fixed t_p of 1 ms is further analyzed. A plot of the calculated V_{dm} as a function of V_p for different values of R_{series} is depicted in Figure 7c. From the plot, the value of V_{dm} appears to change with R_{series}. As mentioned before, the residual voltage drop across the cell after SET further contributes to reducing the resistance of the device, thus increasing the size of the filament, throughout the pulse duration. The magnitude of the device resistance change depends on the amount of the residual voltage drop V_{dm}. This in part explains the second point raised in Section 2.3 regarding the different slopes for different R_{series} values in the $\log(t_r)$–V_p plot (Figure 6).

From Figure 6a, the relaxation time depends on V_p with relatively pronounced slopes for R_{series} of 50 and 100 kΩ. On the other hand, the slopes for the R_{series} of 560 kΩ and 1 MΩ are almost flat, displaying less dependence on V_p. Hence a question arises: what are the reasons for this huge difference in the slopes between the two relatively small (50 kΩ and 100 kΩ) and big (560 kΩ and 1 MΩ) series resistances? To address this, one should start to argue with the electrical conduction mechanism in the two cases. The conduction mechanism in DM cells can be achieved either in galvanic contact with a full closing of the filament between the two electrodes, or in tunnel-gap type, where the current dominantly originates from electron tunneling between the filament tip and the opposing electrode.[23,70] From the calculated cell resistances in Figure 7b, it can be observed that DMs programmed with R_{series} of 560 kΩ and 1 MΩ are gap-type ($R_{dm} >> 1/G_0$, $G_0 \approx 77.5\ \mu S \approx (12.9\ k\Omega)^{-1}$),[71] indicating that a full filament closing was not achieved. Note that for large series resistances, the voltage divider effect occurs much earlier as the cell resistance approaches the value of the R_{series} quite early and most of the applied voltage drops on the R_{series}, reducing the cell voltage V_{dm} close to V_{min}. As a result, no pronounced filament growth is expected after SET regardless of the pulse amplitude and duration. Hence, the filament ruptures quickly and the relaxation becomes fast and almost independent on V_p.

On the other hand, the conductance of the DM with R_{series} of 50 and 100 kΩ is above the quantum point conductance of 1 G_0 (Figure 7b), manifesting a full filament closing and galvanic contact-type electrical conduction. It has been previously shown that once the filament is closed and all the internal physical barriers are overcome, a very small residual voltage of a fraction of V_p is sufficient to maintain further growth of the filament.[54] This explains the longer relaxation time of the DM connected to a 50 kΩ and 100 kΩ series resistor. However, while the voltage drop across the cell within the same R_{series} is almost constant for all voltages (Figure 7c), the magnitude and changing rate (slope) of the relaxation time are different for different V_p and the two series resistances, respectively. This is originated from the high nonlinearity of the SET kinetics where the filament closing time t_{set} decreases exponentially with voltage as is indicated by the steep slope in the $\log(t_{set})$–V plot of Figure 4. A small increase in V_p significantly reduced t_{set}, thus, for a given pulse duration of t_p the shorter the t_{set} (the higher the V_p) the longer is the excess pulse duration after the closing of the filament. In other words, for the same t_p the size of the filament formed at different voltages not only depends on the magnitude of the V_p (electric field strength) but also on the excess pulse time, (t_p–t_{set}) for a given V_p. This especially holds for already closed filaments. However, the influence of this excess pulse duration is determined by the amount of residual voltage drop V_{dm}. The V_{dm} for the R_{series} of 100 kΩ (≈0.18–0.21 V) is smaller than that of 50 kΩ (≈0.23–0.27 V), therefore, the influence of V_{dm} on the filament growth is slightly more pronounced in the latter case. Accordingly, the device with R_{series} of 50 kΩ exhibits a higher t_r with a steeper slope compared to the device with R_{series} of 100 kΩ.

Therefore, considering the effect of t_p and V_{dm}, the true relationship between t_r and V_p can be determined if the t_r is extracted and analyzed at the onset of the SET switching. The minimum pulse width for a successful SET event at a given voltage can be determined by tracing the SET kinetics curve (**Figure 8**a). When pulse durations of t_{p1} up to t_{p5} that are close to the SET kinetics curve across different voltages are chosen for the device programming, the experimentally obtained relaxation time t_r decreases with increasing V_p, as shown in Figure 8b. This confirms the inverse relationship between t_r and V_p as predicted from a physics-based simulation. However, as shown in Figure 6a, the DM cell with the largest R_{series} of 1 MΩ, where the influence of V_{dm} is the lowest, does not reflect the inverse relationship. Note that the t_p in this case is 1 ms, which is orders of magnitude longer than the switching time t_{set} of a few tens of ns to µs at high voltage regimes. That means, although the influence of V_{dm} on further growth of the filament is almost negligible, it cannot be completely ignored (as long as $V_{dm} > V_{min}$ holds), especially if extremely longer than necessary pulses ($t_p >> t_{set}$) are used.

2.5. Implications of the Series Resistor Effect in Device Operation

Despite the attractive energy efficiency, self-relaxation, and thresholding behavior of DMs, the scalability and controllability of the switching times remain a difficult task. Depending on the final target application, sometimes fast relaxation, other times the tunability of t_r becomes more relevant. To achieve fast relaxation it is important to avoid unnecessary excess pulse time ($t_p >> t_{set}$) to prevent further growth after filament closure. There are two ways to do this. First is the implementation of a short pulse that is just long enough to trigger filament closing. As shown in Figure 8, short relaxation times can be achieved in a DM cell if the device is programmed under full consideration of its intrinsic SET kinetics. However, implementing such a programming scheme requires a continuous adaption of t_p for different V_p due to the high non-linearity of the SET kinetics curve. A technically more easy solution toward DM circuits

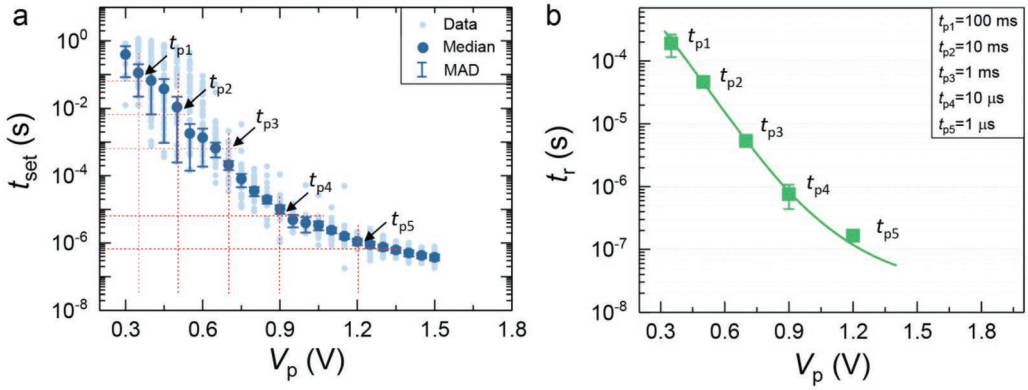

Figure 8. a) SET kinetics data and the selection of different pulse durations t_p that follows the SET kinetics curve. b) A plot of t_r against V_p for different pulse durations defined in (a), displaying the exponential decay of t_r with V_p when short pulses that are long enough to close the filament are used. The solid line in (b) is a guide to the eye and does not represent any physical fitting.

with fast relaxation times is the usage of a proper R_{series}. Thus, unwanted residual voltage drop that might cause uncontrolled filament growth can be diverted to the resistor. This effectively avoids the need to modify t_p every time V_p changes, while still enabling fast relaxation.

The implementation of DMs as a selector in a crossbar array is only feasible if both the SET and relaxation times are short, as fast random access of memory cells within the array is required. Especially, a fast relaxation is essential to effectively prevent current from passing through the unselected cells during operation. However, the existing tradeoff between t_{set} and t_r with respect to V_p and t_p[54] makes it difficult to achieve this goal. Furthermore, as it is revealed in this work, the dependence of t_r on the value of R_{series} makes things even more complicated since adjacent memory cells in a crossbar array could be in LRS, HRS, or in between. Therefore, to make use of DMs as a selector device in a crossbar array, novel concepts and programming techniques such as distributed programming, two-step read scheme,[72] or leveraging the timing of the threshold switching device as shown in Figure 8 and/or suggested in ref. [50] should be adopted.

For neuromorphic applications such as artificial neurons and eligibility trace, however, fast relaxation time is not a necessary prerequisite, rather, the tunability of the relaxation time is more importantly relevant. For example, in a spiking neural network (SNN),[73,74] where DMs can potentially be used as an integrate-and-fire (I&F) neuron,[40,51] the neuronal element is expected to continuously fire with the application of a voltage pulse train. One major challenge is that the DM should relax back to the initial state in the time between the voltage pulses to be ready for the next I&F process.[75,76] Therefore, the gap between the voltage pulses should be longer than the t_r of the DM to guarantee full relaxation. As a result of this, the t_r of the DM cell dictates the maximum firing rate. Thus exploiting ways to control the t_r without affecting the t_{set}—recalling the tradeoff between t_r and t_{set}—is an important step forward in optimizing such devices for neuromorphic computing applications. In this regard, our findings provide a clue on the possibility of using an internal or external series resistor as a means to tune the relaxation time of DMs for applications such as artificial neurons and eligibility trace.

3. Conclusion

In this study, a systematic investigation of the influence of a series resistor on the switching kinetics of Ag/HfO_2/Pt-based diffusive memristor cells is presented. On the one hand, we find no effect of series resistance on the SET kinetics as compared to the stand-alone diffusive memristor. The experimentally observed differences in SET time at higher voltages are mainly due to a capacitive charging time of the complete measurement setup rather than a device property. The limiting processes of the SET kinetics are determined using the analytical approximation of the physics-based device simulation. On the other hand, the relaxation time appears to be significantly affected by the series resistor. It is shown that the dependence of relaxation time on the pulse voltage amplitude can be strongly influenced by the magnitude of the series resistor. Two main reasons responsible for this are: i) the high nonlinearity of the SET-kinetics and ii) the contribution of a residual voltage drop over the device in LRS to the further growth and strengthening of the conductive filament. Furthermore, we discussed the implications of these findings on device operation and exploited ways to tune the relaxation behavior. The understanding of the influence of a series resistance on the switching kinetics of diffusive memristors can contribute to further optimizing the operating condition of diffusive memristors and widen the view of their use as energy-efficient switches in neuromorphic computing.

4. Experimental Section

Fabrication of the Diffusive Memristor Device: The micro-crossbar devices were fabricated on SiO_2/Si with a 430 nm thermally oxidized SiO_2. First, a Ti adhesion layer (5 nm) followed by a Pt (30 nm) bottom electrode was sputtered on the SiO_2/Si substrate. Then, Pt/Ti bottom electrode was lithographically patterned and structured by reactive ion beam etching (RIBE). A homogeneous 3 nm thin HfO_2 insulating film with low defect concentration was grown as a switching layer in a plasma-enhanced atomic layer deposition (PE-ALD) process from tetrakis(ethymethylamino)hafnium (TEMA-Hf) and oxygen plasma at 250 °C.[77,78] Following the switching layer deposition, devices with an area of (3.0 ± 0.2) µm^2 were patterned by photolithography.

Subsequently, crossbar structures were obtained by sputter deposition of an Ag (20 nm) active layer and a Pt (20 nm) capping layer, serving as a top electrode contact, accompanied by a conventional lift-off process. Finally, bottom electrode contacts are opened using photolithography and RIBE.

Device Measurement and Characterization: All electrical characterizations were carried out in a probe station. The voltage sweep electrical measurements were performed by using an Agilent B1500A semiconductor device parameter analyzer equipped with a high-resolution source and measurement units. Transient voltage pulse experiments were carried out by using a Keithley 4200A SCS Semiconductor Characterization System equipped with four 4225 PMUs and an integrated oscilloscope card with a bandwidth of 1 GHz. During all measurements, the bottom Pt-electrode was grounded while the voltage pulse signal was applied to the Pt/Ag top electrode. The applied voltage is measured on channel 1 of the oscilloscope (internal impedance 50 Ω) and the output current can be calculated from the post DUT (Pt counter electrode) signal measured on channel 2 (internal impedance 50 Ω). A custom-built tungsten probe tip was used to introduce the SMD (surface mounted device) resistors used in this work.

Supporting Information

Supporting Information is available from the Wiley Online Library or from the author.

Acknowledgements

This work was in part funded by the German Research Foundation (DFG) under Grant No. SFB 917, in part by the Federal Ministry of Education and Research (BMBF, Germany) in the project NEUROTEC (Project Nos. 16ME0398K and 16ME0399) and NeuroSys (Project No. 03ZU1106AB) and are based on the Jülich Aachen Research Alliance (JARA-FIT). S.A.C. acknowledges the financial support from the DAAD (German Academic Exchange Service). The authors would like to thank Felix Cüppers, Moritz Witzleben, and Stefan Wiefels for fruitful discussions. Technical support of Grigory Potemkin and Clemens Wiedenhöft in sample fabrication and of Marcel Gerst for technical assistance is gratefully acknowledged.

Open access funding enabled and organized by Projekt DEAL.

Conflict of Interest

The authors declare no conflict of interest.

Data Availability Statement

The data that support the findings of this study are available from the corresponding author upon reasonable request.

Keywords

diffusive memristors, electrochemical metallization, relaxation time, switching kinetics, threshold switching, volatile switches

Received: May 16, 2022
Revised: July 8, 2022
Published online: July 28, 2022

[1] J. Backus, *Commun. ACM* **1978**, *21*, 613.
[2] M. A. Zidan, J. P. Strachan, W. D. Lu, *Nat. Electron.* **2018**, *1*, 22.
[3] B. Chen, F. Cai, J. Zhou, W. Ma, P. Sheridan, W. D. Lu, in *2015 IEEE Int. Electron Devices Meeting (IEDM)*, IEEE, Washington, DC **2015**, p. 17.5.1.
[4] C. Mead, *Proc. IEEE* **1990**, *78*, 1629.
[5] S. Yu, B. Gao, Z. Fang, H. Yu, J. Kang, H.-S. P. Wong, in *2012 IEEE Int. Electron Devices Meeting (IEDM 2012)*, IEEE, San Francisco, CA **2012**, p. 10.4.1.
[6] J. Woo, K. Moon, J. Song, S. Lee, M. Kwak, J. Park, H. Hwang, *IEEE Electron Device Lett.* **2016**, *37*, 994.
[7] C. S. Poon, K. Zhou, *Front. Neurosci.* **2011**, *5*, 108/1.
[8] Y. LeCun, Y. Bengio, G. Hinton, *Nature* **2015**, *521*, 436.
[9] J. Y. Seok, S. J. Song, J. H. Yoon, K. J. Yoon, T. H. Park, D. E. Kwon, H. Lim, G. H. Kim, D. S. Jeong, C. S. Hwang, *Adv. Funct. Mater.* **2014**, *24*, 5316.
[10] D.-H. Kwon, K. M. Kim, J. H. Jang, J. M. Jeon, M. H. Lee, G. H. Kim, X.-S. Li, G.-S. Park, B. Lee, S. Han, M. Kim, C. S. Hwang, *Nat. Nanotechnol.* **2010**, *5*, 148.
[11] K. Terabe, T. Hasegawa, T. Nakayama, M. Aono, *Nature* **2005**, *433*, 47.
[12] S. Pi, C. Li, H. Jiang, W. Xia, H. Xin, J. J. Yang, Q. Xia, *Nat. Nanotechnol.* **2019**, *14*, 35.
[13] D. B. Strukov, R. S. Williams, *Proc. Natl. Acad. Sci. USA* **2009**, *106*, 20155.
[14] P. Lin, C. Li, Z. Wang, Y. Li, H. Jiang, W. Song, M. Rao, Y. Zhuo, N. K. Upadhyay, M. Barnell, Q. Wu, J. J. Yang, Q. Xia, *Nat. Electron.* **2020**, *3*, 225.
[15] R. Waser, M. Aono, *Nat. Mater.* **2007**, *6*, 833.
[16] E. Shiu, S. Lim, in *2017 IEEE 9th Int. Memory Workshop (IMW)*, IEEE, Monterey, CA **2017**, p. 1.
[17] R. Waser, R. Dittmann, G. Staikov, K. Szot, *Adv. Mater.* **2009**, *21*, 2632.
[18] H.-S. P. Wong, H.-Y. Lee, S. Yu, Y.-S. Chen, Y. Wu, P.-S. Chen, B. Lee, F. T. Chen, M.-J. Tsai, *Proc. IEEE* **2012**, *100*, 1951.
[19] S. Menzel, U. Böttger, M. Wimmer, M. Salinga, *Adv. Funct. Mater.* **2015**, *25*, 6306.
[20] I. Valov, W. Lu, *Nanoscale* **2016**, *8*, 13828.
[21] R. Fackenthal, M. Kitagawa, W. Otsuka, K. Prall, D. Mills, K. Tsutsui, J. Javanifard, K. Tedrow, T. Tsushima, Y. Shibahara, G. Hush, in *2014 IEEE Int. Solid-State Circuits Conf. Digest of Technical Papers (ISSCC)*, IEEE, San Francisco, CA **2014**, p. 338.
[22] M. N. Kozicki, H. J. Barnaby, *Semicond. Sci. Technol.* **2016**, *31*, 113001/1.
[23] I. Valov, I. Sapezanskaia, A. Nayak, T. Tsuruoka, T. Bredow, T. Hasegawa, G. Staikov, M. Aono, R. Waser, *Nat. Mater.* **2012**, *11*, 530.
[24] C. Schindler, K. Szot, S. Karth&auml, user, R. Waser , *Phys. Status Solidi RRL* **2008**, *2*, 129.
[25] R. Soni, P. Meuffels, G. Staikov, R. Weng, C. Kuegeler, A. Petraru, M. Hambe, R. Waser, H. Kohlstedt, *J. Appl. Phys.* **2011**, *110*, 54509/1.
[26] S. Tappertzhofen, H. Mündelein, I. Valov, R. Waser, *Nanoscale* **2012**, *4*, 3040.
[27] M. Lübben, F. Cüppers, J. Mohr, M. von Witzleben, U. Breuer, R. Waser, C. Neumann, I. Valov, *Sci. Adv.* **2020**, *6*, eaaz9079/1.
[28] T. Tsuruoka, T. Hasegawa, I. Valov, R. Waser, M. Aono, *AIP Adv.* **2013**, *3*, 32114/1.
[29] M. Haemori, T. Nagata, T. Chikyow, *Appl. Phys. Express* **2009**, *2*, 61401/1.
[30] W. Banerjee, S. H. Kim, S. Lee, D. Lee, H. Hwang, *Adv. Electron. Mater.* **2021**, *7*, 2100022/1.
[31] S. H. Choi, S. O. Park, S. Seo, S. Choi, *Sci. Adv.* **2022**, *8*, eabj7866/1.
[32] I. Valov, R. Waser, J. R. Jameson, M. N. Kozicki, *Nanotechnology* **2011**, *22*, 254003/1.

[33] J. Song, J. Woo, S. Lim, S. A. Chekol, H. Hwang, *IEEE Electron Device Lett.* **2017**, *38*, 1532.
[34] N. Gilbert, Y. Zhang, J. Dinh, B. Calhoun, S. Hollmer, in *2013 Symp. On VLSI Circuits*, Kyoto, Japan **2013**, C204.
[35] K.-H. Kim, S. Gaba, D. Wheeler, J. M. Cruz-Albrecht, T. Hussain, N. Srinivasa, W. Lu, *Nano Lett.* **2011**, *12*, 389.
[36] S. Gaba, P. Sheridan, J. Zhou, S. Choi, W. Lu, *Nanoscale* **2013**, *5*, 5872.
[37] S. Lim, C. Sung, H. Kim, T. Kim, J. Song, J. J. Kim, H. Hwang, *IEEE Electron Device Lett.* **2018**, *39*, 312.
[38] J. H. Cha, S. Y. Yang, J. Oh, S. Choi, S. Park, B. C. Jang, W. Ahn, S. Y. Choi, *Nanoscale* **2020**, *12*, 14339.
[39] Z. Wang, S. Joshi, S. E. Savel'ev, H. Jiang, R. Midya, P. Lin, M. Hu, N. Ge, J. P. Strachan, Z. Li, Q. Wu, M. Barne, G. Li, H. L. Xin, R. S. Williams, Q. Xia, J. J. Yang, *Nat. Mater.* **2017**, *16*, 101.
[40] Z. Wang, S. Joshi, S. Savel'ev, W. Song, R. Midya, Y. Li, M. Rao, P. Yan, S. Asapu, Y. Zhuo, H. Jiang, P. Lin, C. Li, J. H. Yoon, N. K. Upadhyay, J. Zhang, M. Hu, J. P. Strachan, M. Barnell, Q. Wu, H. Wu, R. S. Williams, Q. Xia, J. J. Yang, *Nat. Electron.* **2018**, *1*, 137.
[41] M. Wang, W. Wang, W. R. Leow, C. Wan, G. Chen, Y. Zeng, J. Yu, Y. Liu, P. Cai, H. Wang, D. Ielmini, X. Chen, *Adv. Mater.* **2018**, *30*, 1802516/1.
[42] W. Wang, M. Wang, E. Ambrosi, A. Bricalli, M. Laudato, Z. Sun, X. Chen, D. Ielmini, *Nat. Commun.* **2019**, 10, 81.
[43] C. P. Hsiung, H. W. Liao, J. Y. Gan, T. B. Wu, J. C. Hwang, F. Chen, M. J. Tsai, *ACS Nano* **2010**, *4*, 5414.
[44] I. Valov, E. Linn, S. Tappertzhofen, S. Schmelzer, J. v. d. Hurk, F. Lentz, R. Waser, *Nat. Commun.* **2013**, *4*, 1771.
[45] P. Bousoulas, D. Sakellaropoulos, C. Papakonstantinopoulos, S. Kitsios, C. Arvanitis, E. Bagakis, D. Tsoukalas, *Nanotechnology* **2020**, *31*, 454002.
[46] S. Ambrogio, S. Balatti, S. Choi, D. Ielmini, *Adv. Mater.* **2014**, *26*, 3885.
[47] J. Song, J. Woo, A. Prakash, D. Lee, H. Hwang, *IEEE Electron Device Lett.* **2015**, *36*, 681.
[48] Y. Li, J. Tang, B. Gao, W. Sun, Q. Hua, W. Zhang, X. Li, W. Zhang, H. Qian, H. Wu, *Adv. Sci.* **2020**, *7*, 2002251/1.
[49] R. Midya, Z. Wang, J. Zhang, S. E. Savel'ev, C. Li, M. Rao, M. H. Jang, S. Joshi, H. Jiang, P. Lin, K. Norris, N. Ge, Q. Wu, M. Barnell, Z. Li, H. L. Xin, R. S. Williams, Q. Xia, J. J. Yang, *Adv. Mater.* **2017**, *29*, 1604457.
[50] Mingyi Rao, Wenhao Song, Fatemeh Kiani, Shiva Asapu, Ye Zhuo, Rivu Midya, Navnidhi Upadhyay, Qing Wu, Mark Barnell, Peng Lin, Can Li, Zhongrui Wang, Qiangfei Xia, J. Joshua Yang, *Small Sci.* **2022**, *2*, 2100072.
[51] S. A. Chekol, F. Cüppers, R. Waser, S. Hoffmann-Eifert, in *IEEE 2021 IEEE Int. Memory Workshop (IMW)*, IEEE, Dresden, Germany **2021**, pp. 1–4.
[52] J. H. Yoon, Z. Wang, K. M. Kim, H. Wu, V. Ravichandran, Q. Xia, C. S. Hwang, J. J. Yang, *Nat. Commun.* **2018**, *9*, 417/1.
[53] H. Jiang, D. Belkin, S. E. Savel'ev, S. Lin, Z. Wang, Y. Li, S. Joshi, R. Midya, C. Li, M. Rao, M. Barnell, Q. Wu, J. J. Yang, Q. Xia, *Nat. Commun.* **2017**, *8*, 882/1.
[54] S. A. Chekol, S. Menzel, R. W. Ahmad, R. Waser, S. Hoffmann-Eifert, *Adv. Funct. Mater.* **2022**, *32*, 2111242.
[55] U. Böttger, M. von Witzleben, V. Havel, K. Fleck, V. Rana, R. Waser, S. Menzel, *Sci. Rep.* **2020**, *10*, 16391.
[56] K. M. Kim, J. J. Yang, J. P. Strachan, E. M. Grafals, N. Ge, N. D. Melendez, Z. Li, R. S. Williams, *Sci. Rep.* **2016**, *6*, 20085/1.
[57] A. Hardtdegen, C. La Torre, F. Cüppers, S. Menzel, R. Waser, S. Hoffmann-Eifert, *IEEE Trans. Electron Devices* **2018**, *65*, 3229.
[58] T. Liu, M. Verma, Y. Kang, M. Orlowski, *Appl. Phys. Lett.* **2012**, *101*, 073510.
[59] S. Menzel, S. Tappertzhofen, R. Waser, I. Valov, *Phys. Chem. Chem. Phys.* **2013**, *15*, 6945.
[60] E. Gusev, E. Cartier, D. Buchanan, M. Gribelyuk, M. Copel, H. Okorn-Schmidt, C. D'Emic, *Microelectron. Eng.* **2001**, *59*, 341.
[61] J. Robertson, *Eur. Phys. J. Appl. Phys.* **2004**, *28*, 265.
[62] P. K. Park, S. W. Kang, *Appl. Phys. Lett.* **2006**, *89*, 192905/1.
[63] Y. Lin, R. Puthenkovilakam, J. Chang, *Appl. Phys. Lett.* **2002**, *81*, 2041.
[64] H. Harris, K. Choi, N. Mehta, A. Chandolu, N. Biswas, G. Kipshidze, S. Nikishin, S. Gangopadhyay, H. Temkin, *Appl. Phys. Lett.* **2002**, *81*, 1065.
[65] M. Luebben, S. Menzel, S. G. Park, M. Yang, R. Waser, I. Valov, *Nanotechnology* **2017**, *28*, 135205/1.
[66] M. von Witzleben, S. Walfort, R. Waser, S. Menzel, U. Böttger, *IEEE J. Electron Devices Soc.* **2021**, *9*, 667.
[67] Y. Zhuo, R. Midya, W. Song, Z. Wang, S. Asapu, M. Rao, P. Lin, H. Jiang, Q. Xia, R. S. Williams, J. J. Yang, *Adv. Electron. Mater.* **2021**, 2100696.
[68] Y. Li, E. J. Fuller, J. D. Sugar, S. Yoo, D. S. Ashby, C. H. Bennett, R. D. Horton, M. S. Bartsch, M. J. Marinella, W. Lu, A. A. Talin, *Adv. Mater.* **2020**, *32*, 2003984.
[69] Z. Wang, S. Joshi, S. E. Savel'ev, H. Jiang, R. Midya, P. Lin, M. Hu, N. Ge, J. P. Strachan, Z. Li, Q. Wu, M. Barnell, G.-L. Li, H. L. Xin, R. S. Williams, Q. Xia, J. J. Yang, *Nat. Mater.* **2016**, *16*, 101.
[70] S. Menzel, U. Böttger, R. Waser, *J. Appl. Phys.* **2012**, *111*, 014501/1.
[71] E. Scheer, N. Agrait, J. Cuevas, A. Yeyati, B. Ludoph, A. Martin-Rodero, G. Bollinger, J. van Ruitenbeek, C. Urbina, *Nature* **1998**, *394*, 154.
[72] J. Woo, S. Yu, *IEEE Trans. Electron Devices* **2018**, *65*, 5549.
[73] K. Roy, A. Jaiswal, P. Panda, *Nature* **2019**, *575*, 607.
[74] W. Maass, *Neural Networks* **1997**, *10*, 1659.
[75] D. Lee, M. Kwak, K. Moon, W. Choi, J. Park, J. Yoo, J. Song, S. Lim, C. Sung, W. Banerjee, H. Hwang, *Adv. Electron. Mater.* **2019**, *5*, 1800866/1.
[76] X. Zhang, J. Lu, Z. Wang, R. Wang, J. Wei, T. Shi, C. Dou, Z. Wu, J. Zhu, D. Shang, G. Xing, M. Chan, Q. Liu, M. Liu, *Sci. Bull.* **2021**, *66*, 1624.
[77] A. Hardtdegen, H. Zhang, S. Hoffmann-Eifert, *ECS Trans.* **2016**, *75*, 177.
[78] A. C. Dippel, O. Gutowski, L. Klemeyer, U. Boettger, F. Berg, T. Schneller, A. Hardtdegen, S. Aussen, S. Hoffmann-Eifert, M. V. Zimmermann, *Nanoscale* **2020**, *12*, 13103.